The simulation of pantograph and catenary: a PDAE approach

M. ARNOLD* AND B. SIMEON†

ABSTRACT

Recently, the coupled dynamical simulation of pantograph and catenary in high speed trains has found much interest. The equations of motion form a partial differential-algebraic equation (PDAE) that combines a partial differential equation (PDE) for the catenary and a differential-algebraic equation (DAE) for the pantograph. In the present paper we discuss the relation of this PDAE model to current work on the analysis of PDAE's [3, 17, 18] and formulate a benchmark problem to stimulate further research on this topic. The benchmark problem is solved numerically using a semi-discretization in space (by finite elements or finite differences). For time discretization, typical DAE techniques are applied (index reduction, projection steps, handling of systems with varying structure).

Key words: interaction pantograph/catenary, mechanical multibody system, partial differential-algebraic equation (PDAE).

1 INTRODUCTION

The contact between pantograph and catenary is the most critical part in the transmission of electrical energy to modern high-speed trains (e. g. ICE, TGV). The high-speed motion of the pantograph results in oscillations in the contact wire such that the contact force between pantograph and catenary varies strongly and the contact may even get lost. Therefore, special pantographs and catenaries have been developed and further constructive changes are under development. Design criteria include the permanent contact of pantograph head and contact wire at high speed and the reduction of both aeroacoustic noise and wear [20].

Because of the complicated dynamical behaviour and because of very high costs for prototypes, all modifications and new design concepts for the system pantograph/catenary are essentially based on dynamical simulation. Traditional approaches focus on the catenary, which is modelled as set of coupled

*DLR German Aerospace Centre, Institute of Robotics and System Dynamics, P.O. Box 1116, D – 82230 Wessling, Germany. – email: martin.arnold@dlr.de.

†Fachbereich Mathematik, TU Darmstadt, Schloßgartenstr. 7, D – 64289 Darmstadt, Germany. – email: simeon@mathematik.tu-darmstadt.de.

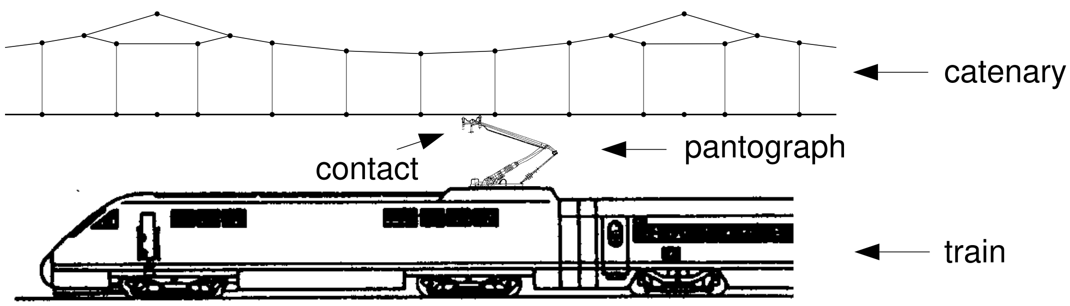

Fig. 1. System pantograph/catenary (see [20, Fig. 1]).

strings and / or beams whereas simplified lumped mass models are used to describe the pantograph. The increased computer power allows nowadays the application of more refined pantograph models considering e. g. the elasticity of the pantograph and active control components in innovative pantograph concepts.

In the present paper we consider the combination of a beam model for the contact wire with a mechanical multibody system (MBS) model for the pantograph. Both substructures are modelled separately resulting in partial differential equations (PDE's, catenary) and differential-algebraic equations (DAE's, pantograph). Because of the geometrical contact between pantograph and contact wire the substructures are coupled. The equations of motion form a partial differential-algebraic equation (PDAE) consisting of the PDE part, the DAE part, and the contact condition that couples PDE and DAE.

The efficient coupled dynamical simulation of pantograph and catenary is per se a challenging problem from the viewpoint of both mechanical engineering and numerics. In the present paper, however, we consider mainly the modelling aspect of the problem.

The analysis and numerical solution of PDAE's has found increasing interest over the last few years. Typical practical applications have their origin in chemical engineering and in structural mechanics. Most work was done in the design and implementation of numerical methods to handle the PDE part (that may in general be expected to cause most of the numerical effort). Theoretical investigations focussed on linear systems with constant coefficients [3, 17, 18]. The definition and development of concepts that are very useful in standard DAE theory (e. g. differentiation index, index reduction, perturbation index [2]) is in the PDAE case still not far beyond its infancy.

Up to now there are not many applied problems that have been considered from the PDAE viewpoint in the literature. The main purpose of the present paper is to provide a simple but nevertheless non-trivial example that has furthermore a strong background in the current development of high-speed trains.

The most common approach to handle the elastic deformation of bodies in a multibody system is based on a Ritz ansatz combined with modal model reduction. The deformation is approximated by a linear combination

$$\sum_{j=1}^{J} q_j(t)\phi_j(\underline{x}) \tag{1}$$

of a small number of eigenmodes $\phi_j(\underline{x})$ corresponding to the very first eigenfrequencies where typically $J \ll 100$ [25]. Choosing a suitable set of eigenmodes $\{\, \phi_j \,:\, 1 \leq j \leq J \,\}$, this approach has been used successfully in many applications and is implemented in modern MBS simulation packages. Since the set of eigenmodes $\{\, \phi_j \,:\, 1 \leq j \leq J \,\}$ is already fixed in the MBS model setup, the equations of motion are reduced from a PDAE (with the PDE part describing the elastic deformation) to a standard DAE before time discretization.

As a consequence, standard DAE–integrators are applied in the dynamical simulation. Eigenmodes $\phi_j(\underline{x})$ corresponding to high eigenfrequencies may cause problems in the time discretization because they introduce stiffness and oscillatory solution components in the equations of motion. In this context, the instability of time discretization schemes and order reduction phenomena have been studied following the lines of stiff ODE theory [22, 23].

For several reasons the system pantograph/catenary does not fit into this classical framework [20]: Measurements show that the pantograph – catenary interaction is essentially influenced not only by low-frequency but also by high-frequency processes. Furthermore, the number of eigenmodes in the frequency range of interest is very large (in a typical application there are $J = 200$ eigenmodes up to 22 Hz [14]). Additional eigenmodes have to be considered if one of the droppers between carrier and contact wire slackens. Because of a reduced numerical effort per time step and because of greater flexibility w. r. t. changes of the system structure, spatial discretizations by finite elements (FEM) or finite differences (FDM) have become an attractive alternative ([21, 20], see also Sec. 4 below).

All these approaches are variants of the method of lines (MOL), i. e. in a first step the PDAE is discretized in space (e. g. by (1), FEM, or FDM) and the resulting (very large) DAE is discretized in time in a separate second step. In general, the time discretization scheme will be adapted to the method being used for space discretization. But there are basic parts of the time integration problem that are common to all approaches and that are studied most conveniently at the original PDAE (index reduction, drift-off effect, ...). A similar situation may be found in the analysis of time integration methods for MOL approximations to parabolic PDE's where order reduction phenomena in implicit Runge–Kutta methods are studied considering the Runge–Kutta time discretization of the parabolic PDE [16].

In our opinion the PDAE approach is natural and useful in the time integration of all MBS models that include elastic effects at higher frequencies. But in the present paper we restrict ourselves to the system pantograph/catenary and to models for pantograph and catenary that are well known from the engineering literature. The remaining part of the paper is organized as follows: In Sec. 2 we describe the mechanical system pantograph/catenary and outline the equations of motion. Furthermore, a simplified benchmark problem that may be used for an analysis of numerical effects is introduced. Sec. 3 deals with the PDAE aspect, in particular with the coupling of both subsystems. The details of space discretization (by FEM and FDM) and time discretization are given in Sec. 4 and in Sec. 5, respectively. At the end we present in Sec. 6 simulation results for the benchmark problem.

2 A MODEL FOR PANTOGRAPH AND CATENARY

In this section we describe some of the details of the technical system and summarize basic model assumptions. The equations of motion of the catenary are outlined following Poetsch et al. [20] while the pantograph is treated as a standard multibody system.

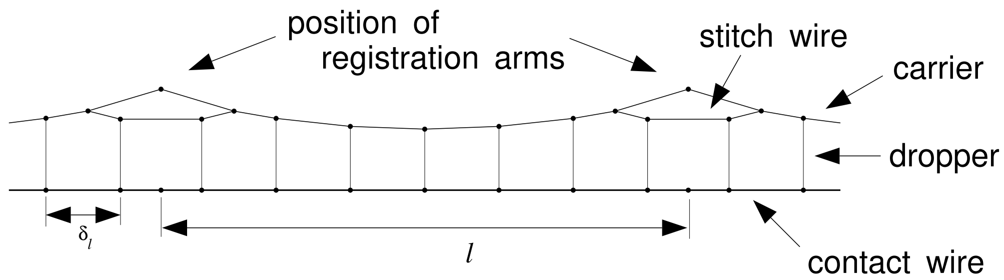

Fig. 2. Basic construction of a stitched wire catenary (adapted from [20, Fig. 2]).

Catenaries are assembled of simple standard elements (e. g. carrier, contact wire, droppers, registration arms, insulators). Fig. 2 shows a part of a stitched wire catenary that is used at German high speed tracks. In intervals of length $l \approx 65.0\,\mathrm{m}$, the carrier and the contact wire are fixed by registration arms. The distance between the droppers connecting carrier and contact wire is $d \approx 9.0\,\mathrm{m}$.

The droppers are designed to suspend the contact wire, they are connected to carrier and contact wire by suspension clamps.

In a catenary without stitch wires the contact force between pantograph and catenary would vary strongly when the pantograph passes a registration arm. Stitch wires were introduced to smooth the contact force. The contact wire (and the complete catenary) is splitted in sections of length $\bar{l} \approx 1200\,\mathrm{m}$, the interactions between subsequent sections are negligible. Therefore, the generic simulation problem is given by the interaction between a catenary of length $\bar{l}$ and a pantograph that moves with fixed speed along the track.

To simplify the presentation we restrict ourselves to a part of this problem and consider instead of a whole section only the region between two subsequent registration arms. In this simplified model the pantograph never passes a registration arm such that it makes sense to neglect the stitch wire. In dimensionless form we end up with the configuration that is shown in Fig. 3: In a region of length L a carrier and a contact wire are connected by n_d droppers at positions $x_{\mathrm{d},j}$. The position of the pantograph at time t is given by $x_\mathrm{p}(t)$.

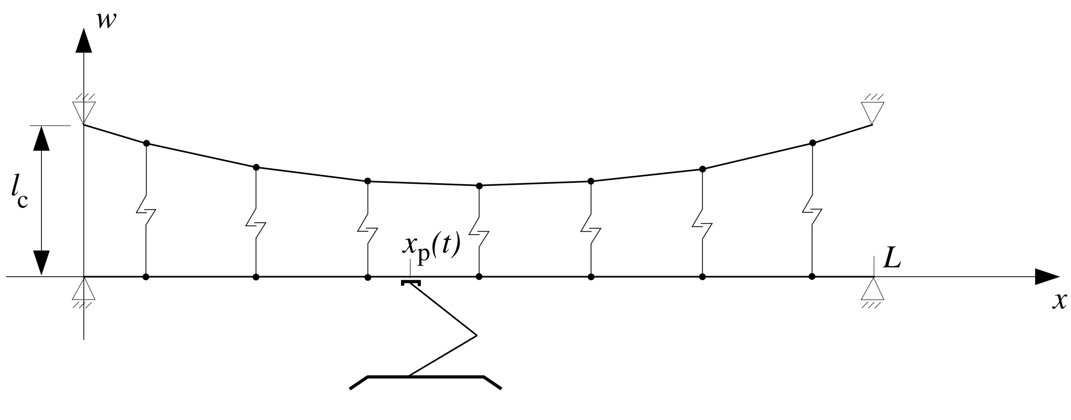

Fig. 3. The reduced catenary model, $L = 65.0$, $n_\mathrm{d} = 7$, $x_{\mathrm{d},j} = 9.0j - 3.5$, $(j = 1, \ldots, n_\mathrm{d})$.

2.1 Equations of motion

The model error and the complexity of the numerical solution depend mainly on the selection of appropriate models for carrier and contact wire. We make the essential model assumption that the displacements in lateral direction are negligible such that the geometric problem dimension is reduced from 3D to 2D. Following this approach, models of increasing complexity have been compared in [20]: strings, Euler–Bernoulli beams, and Timoshenko beams.

Extensive numerical experiments have shown that the carrier may be described by any of these three models. The situation is different for the contact wire because of the moving load induced by the pantograph. The bending stiffness of the contact wire may not be neglected, therefore the string model is not applicable here. To keep the numerical effort small the carrier will be modelled as homogeneous string and the contact wire as Euler–Bernoulli beam such that the vertical displacements $w_{\mathrm{c}}(x,t)$ and $w_{\mathrm{w}}(x,t)$ of **c**arrier and contact **w**ire satisfy

$$\begin{aligned} \varrho_{\mathrm{c}} A_{\mathrm{c}} \ddot{w}_{\mathrm{c}} + \beta_{\mathrm{c}} \dot{w}_{\mathrm{c}} &= T_{\mathrm{c}} w_{\mathrm{c}}'' - \varrho_{\mathrm{c}} A_{\mathrm{c}} g - \sum_{j=1}^{n_{\mathrm{d}}} f_{\mathrm{d},j}^{\mathrm{c}} \,, \\ \varrho_{\mathrm{w}} A_{\mathrm{w}} \ddot{w}_{\mathrm{w}} + \beta_{\mathrm{w}} \dot{w}_{\mathrm{w}} &= -E_{\mathrm{w}} I_{\mathrm{w}} w_{\mathrm{w}}'''' + T_{\mathrm{w}} w_{\mathrm{w}}'' - \varrho_{\mathrm{w}} A_{\mathrm{w}} g - \sum_{j=1}^{n_{\mathrm{d}}} f_{\mathrm{d},j}^{\mathrm{w}} + f_{\mathrm{p}}^{\mathrm{w}} \end{aligned} \tag{2}$$

with boundary conditions

$$\begin{aligned} w_{\mathrm{c}}(0,t) = w_{\mathrm{c}}(L,t) = l_{\mathrm{c}} \,, \\ w_{\mathrm{w}}(0,t) = w_{\mathrm{w}}(L,t) = 0 \,, \;\; w_{\mathrm{w}}''(0,t) = w_{\mathrm{w}}''(L,t) = 0 \,. \end{aligned} \tag{3}$$

The physical parameters of **c**arrier and contact **w**ire are denoted by ϱA (mass per unit length), T (tensile force), EI (bending stiffness), and g (gravitational acceleration) while viscous damping is determined by the parameter β. The droppers and the contact between pantograph and catenary result in the loads $f_{\mathrm{d},j}^{\mathrm{c}}$, $f_{\mathrm{d},j}^{\mathrm{w}}$, and $f_{\mathrm{p}}^{\mathrm{w}}$.

The droppers are modelled as wires of fixed length l_j, the mass per unit length is denoted by $\varrho_{\mathrm{d}} A_{\mathrm{d}}$. The suspension clamps are considered as point masses m_{s} that are attached to carrier and contact wire at position $x_{\mathrm{d},j}$. Thus, the loads $f_{\mathrm{d},j}$, $(j = 1,\ldots,n_{\mathrm{d}})$ in (2) are given by

$$\begin{aligned} f_{\mathrm{d},j}^{\mathrm{c}}(x,t) &= \delta(x - x_{\mathrm{d},j}) \cdot ((m_{\mathrm{s}} + \tfrac{1}{2} l_j \varrho_{\mathrm{d}} A_{\mathrm{d}}) g + \lambda_{\mathrm{d},j}(t)) \\ f_{\mathrm{d},j}^{\mathrm{w}}(x,t) &= \delta(x - x_{\mathrm{d},j}) \cdot ((m_{\mathrm{s}} + \tfrac{1}{2} l_j \varrho_{\mathrm{d}} A_{\mathrm{d}}) g - \lambda_{\mathrm{d},j}(t)) \end{aligned} \tag{4}$$

with the Dirac function δ and constraint forces $\lambda_{\mathrm{d},j}(t) \geq 0$ that guarantee that the unilateral constraints

$$\Delta_{\mathrm{d},j}(t) := w_{\mathrm{w}}(x_{\mathrm{d},j},t) - w_{\mathrm{c}}(x_{\mathrm{d},j},t) + l_j \geq 0 \tag{5}$$

are always satisfied. In nominal position all n_{d} unilateral constraints (5) are active (i. e. $\Delta_{\mathrm{d},j}(t) = 0$) but they may get inactive if one of the droppers slackens during simulation. An inactive constraint corresponds to a vanishing constraint force such that we get complementarity conditions

$$\lambda_{\mathrm{d},j}(t) \cdot \Delta_{\mathrm{d},j}(t) = 0 \,, \;\; (j = 1,\ldots,n_{\mathrm{d}}) \tag{6}$$

(see e. g. [15] for an extensive discussion of unilateral constraints in standard DAE theory).

In (4), the loads are concentrated in isolated points $x_{\mathrm{d},j}$ that are *fixed* during integration and correspond in a natural way to a fixed element or fixed grid point if FEM or FDM are used for space discretization. The contact between pantograph and catenary, on the other hand, results in a *moving point force* acting in an isolated point $x_{\mathrm{p}}(t)$. Thus, the force term $f_{\mathrm{p}}^{\mathrm{w}}$ of (2) is given by

$$f_{\mathrm{p}}^{\mathrm{w}}(x,t) = \delta(x - x_{\mathrm{p}}(t))\,\lambda_{\mathrm{p}}(t)\ , \tag{7}$$

and the geometrical contact condition of pantograph and catenary reads

$$\Delta_{\mathrm{p}}(t) := w_{\mathrm{w}}(x_{\mathrm{p}}(t),t) - b(t, q_{\mathrm{MBS}}(t)) \geq 0\ . \tag{8}$$

Here, $b(t, q_{\mathrm{MBS}})$ denotes the vertical position of the pantograph head depending on the position coordinates q_{MBS} of the pantograph. Again, we have a complementarity condition

$$\lambda_{\mathrm{p}}(t) \cdot \Delta_{\mathrm{p}}(t) = 0\ . \tag{9}$$

At the moment we do not specify a detailed pantograph model and suppose only that its position may be completely described by coordinates q_{MBS} that satisfy the standard MBS model equations [5]

$$\begin{aligned} M_{\mathrm{MBS}}(q_{\mathrm{MBS}})\ddot{q}_{\mathrm{MBS}} &= f_{\mathrm{MBS}}(t, q_{\mathrm{MBS}}, \dot{q}_{\mathrm{MBS}}) + G_{\mathrm{MBS}}^T(t, q_{\mathrm{MBS}})\lambda_{\mathrm{MBS}} - B^T(t, q_{\mathrm{MBS}})\lambda_{\mathrm{p}}\ , \\ 0 &= g_{\mathrm{MBS}}(t, q_{\mathrm{MBS}}) \end{aligned} \tag{10}$$

with mass matrix $M_{\mathrm{MBS}}(q_{\mathrm{MBS}})$, holonomic constraints $g_{\mathrm{MBS}} = 0$, and force terms that contain the internal constraint forces $G_{\mathrm{MBS}}^T\lambda_{\mathrm{MBS}}$ of the pantograph where $G_{\mathrm{MBS}} := \frac{\partial}{\partial q_{\mathrm{MBS}}} g_{\mathrm{MBS}}(t, q_{\mathrm{MBS}})$.

The second constraint force term

$$-B^T(t, q_{\mathrm{MBS}})\lambda_{\mathrm{p}} \quad \text{with} \quad B := \frac{\partial b}{\partial q_{\mathrm{MBS}}}(t, q_{\mathrm{MBS}}) \tag{11}$$

results from the interaction with the catenary. Summing up, the model for the system pantograph/catenary is completely described by (2)–(11).

2.2 A simplified benchmark problem

In real life applications, the dynamical simulation of the interaction between pantograph and catenary requires a very large numerical effort. We introduce in this subsection a simplified benchmark problem in order to discuss the basic steps of discretization in space and time.

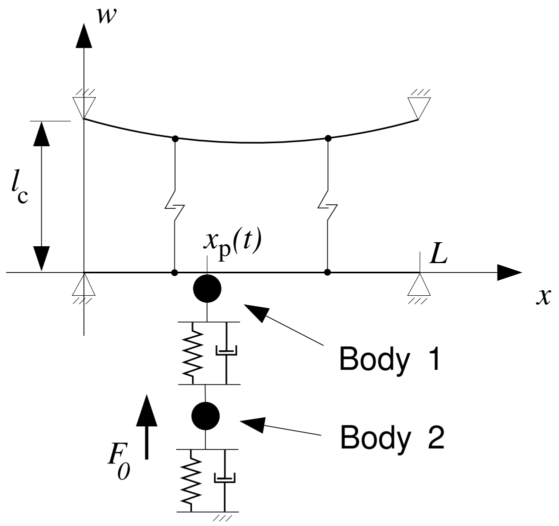

Fig. 4. Geometry of the model problem.

For the benchmark problem, we consider the interaction between a simplified catenary with only $n_{\mathrm{d}} = 2$ droppers and a lumped mass model for the pantograph. The "pantograph" consists of two point masses representing the pantograph head (Body 1) and the remaining parts of the pantograph (Body 2). There are spring–damper elements between Bodies 1 and 2 and between Body 2 and the ground (see Fig. 4). Both bodies move with fixed speed v_{p} in x-direction such that $x_{\mathrm{p}}(t)$ in (7) is given by

$$x_{\mathrm{p}}(t) = x_{\mathrm{p},0} + v_{\mathrm{p}} t \ .$$

The contact pressure of the pantograph and the gravitational forces are modelled by a constant force F_0 acting on Body 2 in vertical direction.

With this simplified model we have

$$q_{\mathrm{MBS}} = (\, w_{\mathrm{p},1} \,,\, w_{\mathrm{p},2} \,)^T \ , \quad b(t, q_{\mathrm{MBS}}) = w_{\mathrm{p},1}$$

and (10) gets the form

$$\begin{aligned} m_1 \ddot{w}_{\mathrm{p},1} &= -d_1(\dot{w}_{\mathrm{p},1} - \dot{w}_{\mathrm{p},2}) - c_1(w_{\mathrm{p},1} - w_{\mathrm{p},2}) - \lambda_{\mathrm{p}}(t) \\ m_2 \ddot{w}_{\mathrm{p},2} &= -d_2 \dot{w}_{\mathrm{p},2} + d_1(\dot{w}_{\mathrm{p},1} - \dot{w}_{\mathrm{p},2}) - c_2 w_{\mathrm{p},2} + c_1(w_{\mathrm{p},1} - w_{\mathrm{p},2}) + F_0 \end{aligned} \qquad (12)$$

with $w_{\mathrm{p},j}$ denoting the w-coordinate of Body j.

The simulation results of Sec. 6 illustrate that this simplified model reflects qualitatively typical effects of the real technical system. As a drawback of this configuration we observed in the numerical tests that the simulation results depend strongly on the initial conditions. The influence of the initial state is dominating in the beginning of the motion, only after some seconds it is negligible because of damping. Therefore the initial conditions for the model problem are adjusted carefully to avoid artefacts like frequent slackening of droppers.

In the subsystem "catenary" we start with a stationary state:

$$\dot{w}_{\mathrm{c}}(x,0) = \dot{w}_{\mathrm{w}}(x,0) = \ddot{w}_{\mathrm{c}}(x,0) = \ddot{w}_{\mathrm{w}}(x,0) = 0\ , \quad 0 \le x \le L\ .$$

These conditions define for any given load $f_{\mathrm{p}}^{\mathrm{w}}$ the displacements $w_{\mathrm{c}}(x,0)$ and $w_{\mathrm{w}}(x,0)$ as solution of an elliptic system (2) with boundary conditions (3) and constraints (5). In the subsystem "pantograph" we assume

$$w_{\mathrm{p},1}(0) = w_{\mathrm{p},2}(0) \tag{13}$$

and suppose furthermore that pantograph and catenary are in contact at $t = 0$. Then the contact condition, the hidden constraints (see Sec. 4.1 below), and (12) define the initial values of $w_{\mathrm{p},j}$, $\dot{w}_{\mathrm{p},j}$, $\ddot{w}_{\mathrm{p},j}$, $(j = 1,2)$.

Following Poetsch et al. [20] (see also [19, Appendix O]) the material dependent constants in the catenary model are adapted to measured data for the catenary `Re 250` of the Deutsche Bahn AG: The masses per unit length are $\varrho_{\mathrm{c}} A_{\mathrm{c}} = 0.6\,\mathrm{kg/m}$, $\varrho_{\mathrm{w}} A_{\mathrm{w}} = 1.068\,\mathrm{kg/m}$, $\varrho_{\mathrm{d}} A_{\mathrm{d}} = 0.14\,\mathrm{kg/m}$, the damping constants are $\beta_{\mathrm{c}} = \beta_{\mathrm{w}} = 0.03\,\mathrm{Ns/m^2}$, the tensile forces are $T_{\mathrm{c}} = T_{\mathrm{w}} = 15.0\,\mathrm{kN}$ and the bending stiffness of the contact wire is given by $E_{\mathrm{w}} I_{\mathrm{w}} = 150.0\,\mathrm{Nm^2}$. The suspension clamps have mass $m_{\mathrm{s}} = 0.25\,\mathrm{kg}$, and the actually used constant of gravity is $g = 9.81\,\mathrm{m/s^2}$.

The geometry of the model problem is defined by the length $L = 20.0\,\mathrm{m}$ of the "catenary", by the distance $l_{\mathrm{c}} = 1.0\,\mathrm{m}$ between carrier and contact wire at $x = 0$ and $x = L$ and by the positions $x_{\mathrm{d},1} = 5.5\,\mathrm{m}$, $x_{\mathrm{d},2} = 14.5\,\mathrm{m}$ and the length $l_1 = l_2 = 0.95\,\mathrm{m}$ of the two droppers.

Lumped mass models for the pantograph have been considered frequently in the literature (see e. g. [19, Sec. 4]). We use a set of parameters that goes back to Fischer [6]: $m_1 = 9.0\,\mathrm{kg}$, $m_2 = 17.0\,\mathrm{kg}$, $c_1 = 7000.0\,\mathrm{N/m}$, $c_2 = 0.0\,\mathrm{N/m}$, $d_1 = 30.0\,\mathrm{Ns/m}$, $d_2 = 130.0\,\mathrm{Ns/m}$, $F_0 = 70.0\,\mathrm{N}$. The initial position of the "pantograph" is $x_{\mathrm{p},0} = x_{\mathrm{p}}(0) = 2.0\,\mathrm{m}$, the simulation is stopped if the end position $x_{\mathrm{p}}(t_e) = 18.0\,\mathrm{m}$ has been reached. The initial constraint force between pantograph and catenary is set to $\lambda_{\mathrm{p}}(0) := 8.75\,\mathrm{N}$.

3 REFORMULATION AS PDAE PROBLEM

In this section, we want to discuss the pantograph catenary model from above in more detail and finally reformulate it as a mixed system of PDE's and DAE's or "PDAE", a term which has not yet been exactly defined in the literature. It was introduced to characterize coupled systems of PDE's, ODE's and / or DAE's that contain (explicitly or implicitly) relations which do not involve time derivatives of the solution. A typical example is the incompressibility condition $\nabla \cdot u(x,t) = 0$ in the Navier–Stokes equations (see e. g. [2, (1.3.14)]).

Up to now, the work on PDAE's has focussed on the special case that these relations have to be satisfied *pointwise* for all t and x of the time interval and the spatial domain of interest (see [3, 4, 17] and the references therein). The Navier–Stokes equations fit into this class of PDAE's. On the other hand, constraints in mechanical systems are very often formulated for isolated spatial points or parts of the boundary or some subdomain. The pantograph/catenary model is an instructive example for this class of constrained PDE's or PDAE's.

3.1 Moving point force and constraint formulation

Since the whole model of Sec. 2 shows a rather complex structure, we first concentrate on only one PDE subject to one time dependent constraint. Consider the beam equation

$$\varrho A \ddot{w} = -EIw'''' + Tw'' - \varrho A g \tag{14}$$

with boundary conditions as in (3). In case of an equality constraint, the contact condition (8) leads basically to a PDAE of type

$$\begin{aligned} \varrho A \ddot{w} &= -EIw'''' + Tw'' - \varrho A g + \delta(x - x_{\mathrm{p}}(t))\, \lambda_{\mathrm{p}}(t) \\ 0 &= w(x_{\mathrm{p}}(t), t) - b(t) \end{aligned} \tag{15}$$

where we assumed b to be a known function to simplify matters. The corresponding weak form reads, for all testfunctions $v : [0, L] \to \mathbb{R}$ satisfying the boundary conditions,

$$\begin{aligned} \varrho A \textstyle\int v \ddot{w}\, \mathrm{d}x &= -EI \textstyle\int v''w''\mathrm{d}x - T \textstyle\int v'w'\mathrm{d}x - \varrho A g \textstyle\int v\, \mathrm{d}x + v(x_{\mathrm{p}})\, \lambda_{\mathrm{p}}(t)\ , \\ 0 &= w(x_{\mathrm{p}}, t) - b(t)\ . \end{aligned} \tag{16}$$

The integrals range here from 0 to L. In general, the Sobolev space H_0^2 will be appropriate for such a beam model [1] while H_0^1 is the basic setting in case of the string ($EI = 0$).

As an alternative to the point constraint in (15), the displacement of the wire can also be prescribed in an interval or subdomain $I = [x_{\mathrm{p}} - \epsilon, x_{\mathrm{p}} + \epsilon]$. In weak form, we obtain then

$$\begin{aligned} \varrho A \int v\ddot{w}\,\mathrm{d}x &= -EI\int v''w''\mathrm{d}x - T\int v'w'\mathrm{d}x - \varrho Ag\int v\,\mathrm{d}x + \int_I v(x)\Lambda(x,t)\,\mathrm{d}x\ , \\ 0 &= \int_I \mu(x)(w(x,t)-b(t))\,\mathrm{d}x\ . \end{aligned} \tag{17}$$

Now, a Lagrange multiplier $\Lambda(x,t)$ appears which depends on both space and time, and the constraint is only formulated in a weak sense with test functions μ. Eqs. (17) are directly related to constraint variational and saddle point problems, see, e. g., Kikuchi/Oden [13] for more details.

Though the above constrained PDE's show some formal similarities to DAE's, it turns out that they feature much different properties. We illustrate that by calculating the Lagrange multiplier λ_p of (15). In standard DAE theory, one would differentiate the constraints twice with respect to time in order to derive an algebraic expression in λ_p (see e. g. [11, (VII.1.46e)]). Here, we start with the formal differentiation

$$\frac{\mathrm{d}^2}{\mathrm{d}t^2}w(x(t),t) = w''\dot{x}^2 + 2\dot{w}'\dot{x} + w'\ddot{x} + \ddot{w} \tag{18}$$

where $\dot{w} = \partial w/\partial t$. The balance of momentum for a control volume moving along with the contact point $x_\mathrm{p}(t)$ yields

$$\int_{x_\mathrm{p}-\epsilon}^{x_\mathrm{p}+\epsilon} \varrho A\frac{\mathrm{d}^2}{\mathrm{d}t^2}w(x(t),t)\,\mathrm{d}x = \int_{x_\mathrm{p}-\epsilon}^{x_\mathrm{p}+\epsilon}(-EIw'''' + Tw'' - \varrho Ag)\,\mathrm{d}x + \lambda_\mathrm{p}(t)\ . \tag{19}$$

In case of an Euler-Bernoulli beam, w'' as well as $\dot{w}'$ and $\ddot{w}$ are still continuous but w''' has a discontinuity at x_p. Hence, for the limit case $\epsilon \to 0$ all integrals in the balance equation (19) vanish except for the bending term, which leads to

$$\lambda_\mathrm{p}(t) = EI(w'''(x_\mathrm{p}^+,t) - w'''(x_\mathrm{p}^-,t))\ . \tag{20}$$

The relation (20) is sometimes called a *compatibility condition* [20] for the moving point force λ_p. In string models ($EI = 0$), even w' is discontinuous at x_p, and thus the derivatives of (18) exist only in subintervals $[x_\mathrm{p}-\epsilon, x_\mathrm{p}^-]$ and $[x_\mathrm{p}^+, x_\mathrm{p}+\epsilon]$. Consequently, the limit case $\epsilon \to 0$ results in a condition which takes the velocity $\dot{x}_\mathrm{p}$ into account [19, Sec. 3],

$$\lambda_\mathrm{p}(t) = (\varrho A\dot{x}_\mathrm{p}^2 - T)(w'(x_\mathrm{p}^+,t) - w'(x_\mathrm{p}^-,t))\,. \tag{21}$$

In standard DAE theory, a given DAE may be transformed to an analytically equivalent one substituting constraints by their time derivatives (typically this substitution is used to reduce the index analytically [8]). Eq. (21) illustrates that this approach can not be carried over to the PDAE model (15) since the point constraint $0 = w(x_\mathrm{p},t) - b(t)$ is in general not differentiable. The situation changes if we pass to the subdomain constraint in (17) where w is smooth inside the intervall I.

3.2 Reformulating the full system

We now turn back to the equations of motion outlined in Sec. 2 and reformulate them as a PDAE system. As long as the time interval of interest may be split in a finite number of sub-intervals $[t_i, t_{i+1}]$ such that the set of active unilateral constraints (5), (8) remains fixed for all $t \in [t_i, t_{i+1}]$, the analysis of the equations of motion is restricted most conveniently to one of these sub-intervals [15]. For ease of presentation, we therefore consider in the following a sub-interval $[t_0, T]$ with all unilateral constraints (5), (8) being active for all $t \in [t_0, T]$. With minor modifications this analysis may be carried over to sub-intervals with inactive constraints.

In $[t_0, T]$ the constraints (5) and (8) define $n_{\rm d} + 1$ functionals that vanish identically for $t \in [t_0, T]$. These functionals are linear in $w_{\rm c}$ and $w_{\rm w}$, they are mappings from a function space to $\mathbb{R}$. We summarize these $n_{\rm d} + 1$ constraints in

$$0 = C_{\rm c} w_{\rm c} + C_{\rm w}(x_{\rm p}(t)) w_{\rm w} - \begin{pmatrix} 0 \\ b(t, q_{\rm MBS}) \end{pmatrix} - z =: g_{\rm PDE}(t, w_{\rm c}, w_{\rm w}, q_{\rm MBS}). \quad (22)$$

The corresponding force terms in (2) and (10) are written as

$$\begin{pmatrix} -\sum_j \delta(x - x_{{\rm d},j}) \lambda_{{\rm d},j}(t) \\ \sum_j \delta(x - x_{{\rm d},j}) \lambda_{{\rm d},j}(t) + f_{\rm p}^{\rm w} \\ -B^T(t, q_{\rm MBS}) \lambda_{\rm p}(t) \end{pmatrix} =: \begin{pmatrix} C_{\rm PDE}^T(x_{\rm p}(t)) \\ C_{\rm MBS}^T(t, q_{\rm MBS}) \end{pmatrix} \lambda_{\rm PDE}(t)$$

with forces $\lambda_{\rm PDE}(t) := (\lambda_{{\rm d},1}, \ldots, \lambda_{{\rm d},n_{\rm d}}, \lambda_{\rm p})^T$ and matrices $C_{\rm PDE} \in \mathbb{R}^{(n_{\rm d}+1)\times 2}$ and $C_{\rm MBS} \in \mathbb{R}^{(n_{\rm d}+1)\times 1}$.

With these notations, (2)–(11) get the compact form

$$\begin{aligned} M(q)\ddot{q} &= A[q] + f(t, q, \dot{q}) + G^T(t, q)\lambda \\ 0 &= g(t, q) \end{aligned} \quad (23)$$

where

$$q := \begin{pmatrix} w_{\rm c}(x,t) \\ w_{\rm w}(x,t) \\ q_{\rm MBS}(t) \end{pmatrix} \ , \quad \lambda := \begin{pmatrix} \lambda_{\rm PDE}(t) \\ \lambda_{\rm MBS}(t) \end{pmatrix} \ ,$$

$$M(q) := \mathrm{blockdiag}(\, \varrho_{\rm c} A_{\rm c} \, , \, \varrho_{\rm w} A_{\rm w} \, , \, M_{\rm MBS}(q_{\rm MBS}) \,) \ ,$$

$$g(t, q) := \begin{pmatrix} g_{\rm PDE}(t, w_{\rm c}, w_{\rm w}, q_{\rm MBS}) \\ g_{\rm MBS}(t, q_{\rm MBS}) \end{pmatrix} \ ,$$

$$G^T(t, q) := \begin{pmatrix} \begin{matrix} C_{\rm PDE}^T(x_{\rm p}(t)) \\ C_{\rm MBS}^T(t, q_{\rm MBS}) \end{matrix} & 0 \\ 0 & G_{\rm MBS}^T(t, q_{\rm MBS}) \end{pmatrix} \ .$$

Furthermore, A denotes the linear differential operator

$$A[q] := \begin{pmatrix} T_{\mathrm{c}} w_{\mathrm{c}}'' \\ -E_{\mathrm{w}} I_{\mathrm{w}} w_{\mathrm{w}}'''' + T_{\mathrm{w}} w_{\mathrm{w}}'' \\ 0 \end{pmatrix} \tag{24}$$

and

$$f(t,q,\dot{q}) := \begin{pmatrix} -\beta_{\mathrm{c}}\dot{w}_{\mathrm{c}} - \varrho_{\mathrm{c}} A_{\mathrm{c}} g - \sum_j \delta(x - x_{\mathrm{d},j})(m_{\mathrm{s}} + \frac{1}{2} l_j \varrho_{\mathrm{d}} A_{\mathrm{d}} g) \\ -\beta_{\mathrm{w}}\dot{w}_{\mathrm{w}} - \varrho_{\mathrm{w}} A_{\mathrm{w}} g - \sum_j \delta(x - x_{\mathrm{d},j})(m_{\mathrm{s}} + \frac{1}{2} l_j \varrho_{\mathrm{d}} A_{\mathrm{d}} g) \\ f_{\mathrm{MBS}}(t, q_{\mathrm{MBS}}, \dot{q}_{\mathrm{MBS}}) \end{pmatrix}$$

contains generalized centrifugal and Coriolis forces and applied forces.

As mentioned at the beginning of this section, the constraints in (23) are *not* pointwise w. r. t. x but they guarantee that certain *functionals* of the solution vanish for all $t \in [t_0, T]$. To the knowledge of the authors, PDAE's of this basic type have not been considered before in the PDAE literature. They are worth to be studied in more detail because coupling conditions between substructures in complex models result typically in this kind of constraints, in particular in a broad class of mechanical systems.

4 SPACE DISCRETIZATION

We turn now to numerical simulation techniques and concentrate in this section on semi-discretization in space by finite elements and finite differences. Before, however, it is necessary to study the contact of pantograph head and contact wire in more detail. The discussion is restricted to the setting of the benchmark problem of Sec. 2.2.

4.1 Moving point forces

Moving point forces are known to cause numerical problems whenever $x_{\mathrm{p}}(t)$ crosses a grid point of a FEM or FDM discretization. We therefore follow the approach (17) and consider explicitly the distribution of the load in the contact area between contact wire and pantograph head (a typical head consists of 2 contact strips spanning a contact area of length $\approx 0.4\,\mathrm{m}$):

$$f_{\mathrm{p}}^{\mathrm{w}}(x,t) = \delta_\epsilon(x - x_{\mathrm{p}}(t))\,\lambda_{\mathrm{p}}(t)\ . \tag{25}$$

In (25) the influence of the actual displacements $w_{\mathrm{w}}(x,t)$ on $f_{\mathrm{p}}^{\mathrm{w}}$ is neglected, the load distribution is described by a normalized function $\delta_\epsilon \in \mathcal{C}^1(-\infty,\infty)$

that is non-negative and vanishes identically outside of $[-\epsilon, \epsilon]$ (here ϵ denotes a small positive parameter),

$$\delta_\epsilon(\xi) \geq 0\ , \quad (\xi \in \mathbb{R})\ , \qquad \int_{-\infty}^{\infty} \delta_\epsilon(\xi)\,\mathrm{d}\xi = 1\ , \qquad \operatorname{supp}\delta_\epsilon = [-\epsilon, \epsilon]\ .$$

In the numerical tests we set $\epsilon := 0.2\,\mathrm{m}$ and use a cubic $\mathcal{C}^1$–spline δ_ϵ with knots $-\epsilon$, 0, and ϵ that satisfies $\delta_\epsilon'(0) = 0$. The analytical expression is obtained straightforwardly as

$$\delta_\epsilon(\xi) := \frac{1}{\epsilon} - 3\frac{\xi^2}{\epsilon^3} + 2\frac{|\xi|^3}{\epsilon^4}\ , \quad \text{if } |\xi| \leq \epsilon\ .$$

The geometrical contact condition pantograph/catenary is formulated consistently with (25):

$$\Delta_\mathrm{p}(t) := \int_{-\infty}^{\infty} \delta_\epsilon(x - x_\mathrm{p}(t))\, w_\mathrm{w}(x,t)\,\mathrm{d}x - b(t, q_\mathrm{MBS}(t)) \geq 0\ . \tag{26}$$

Again, we have the complementarity condition (9).

As long as this contact condition (26) is active the solution of the PDAE has to satisfy additionally the *hidden constraint*

$$0 = \frac{\mathrm{d}}{\mathrm{d}t}\Delta_\mathrm{p}(t) = \int_{-\infty}^{\infty} (-\delta_\epsilon'(x - x_\mathrm{p})\,\dot{x}_\mathrm{p}\, w_\mathrm{w} + \delta_\epsilon(x - x_\mathrm{p})\,\dot{w}_\mathrm{w})\,\mathrm{d}x - b_t - b_q \dot{q}_\mathrm{MBS}$$

on the level of velocity coordinates and the hidden constraint $0 = \frac{\mathrm{d}^2}{\mathrm{d}t^2}\Delta_\mathrm{p}(t)$ on the level of accelerations (similar to standard DAE theory [11, pp. 463ff], see also Sec. 3.1 of the present paper).

4.2 Semi-discretization by finite elements

Let $0 = x_0 < x_1 < \ldots < x_N < x_{N+1} = L$ denote an equidistant grid with $N+1$ subintervals of length $\Delta x = L/(N+1)$ and assume that the dropper positions $x_{\mathrm{d},j}, j = 1, 2$, coincide with some grid points. In each subinterval $[x_i, x_{i+1}]$, the displacements w_c and w_w are approximated by a linear and a cubic Hermite ansatz, respectively,

$$w_\mathrm{c}(x,t) \doteq (1-\xi) q_{\mathrm{c},i}(t) + \xi q_{\mathrm{c},i+1}(t)\ , \quad w_\mathrm{w}(x,t) \doteq \sum_{j=0}^{3} \mathcal{N}_j(x)\, q_{\mathrm{w},2i+j}(t) \tag{27}$$

where $\xi := (x - x_i)/\Delta x$ and the latter shape functions read

$$\begin{aligned} \mathcal{N}_0(x) &= (1-\xi)^2(1+2\xi), & \mathcal{N}_1(x) &= \xi(1-\xi)^2\Delta x, \\ \mathcal{N}_2(x) &= \xi^2(3-2\xi), & \mathcal{N}_3(x) &= -\xi^2(1-\xi)\Delta x\,. \end{aligned}$$

Note, that the coefficients $q_{\mathrm{c},i}$ and $q_{\mathrm{c},i+1}$ approximate w_{c} at nodes x_i and x_{i+1}, $i = 0,\dots,N$, while the coefficients $q_{\mathrm{w},2i+j}$, $j = 0,\dots,3$ approximate both nodal displacements and corresponding spatial derivatives of w_{w}.

If the boundary conditions $w_{\mathrm{c}}(x_0,t) = w_{\mathrm{c}}(x_{N+1},t) = l_{\mathrm{c}}$ and $w_{\mathrm{w}}(x_0,t) = w_{\mathrm{w}}(x_{N+1},t) = 0$ are taken into account, these conforming finite elements of class $\mathcal{C}^0$ and $\mathcal{C}^1$ define in the usual way N global test functions $v_{\mathrm{c}}(x)$ for the carrier and $2N+2$ test functions $v_{\mathrm{w}}(x)$ for the contact wire [24]. Thus, the global approximation can be written as

$$w_{\mathrm{c}}(x,t) \doteq \sum_{j=1}^{N} v_{\mathrm{c},j}(x) q_{\mathrm{c},j}(t)\,, \quad w_{\mathrm{w}}(x,t) \doteq \sum_{j=1}^{2N+2} v_{\mathrm{w},j}(x) q_{\mathrm{w},j}(t)\,. \tag{28}$$

Inserting (28) in the weak form of (2), cf. also (17), and applying all testfunctions, we obtain the semidiscretized equations of motion

$$\begin{aligned} M_{\mathrm{c}}\ddot{q}_{\mathrm{c}} + D_{\mathrm{c}}\dot{q}_{\mathrm{c}} &= -S_{\mathrm{c}}q_{\mathrm{c}} + b_{\mathrm{c}} - H_{\mathrm{c}}^T\lambda_{\mathrm{d}} && (29)\\ M_{\mathrm{w}}\ddot{q}_{\mathrm{w}} + D_{\mathrm{w}}\dot{q}_{\mathrm{w}} &= -(S_{\mathrm{w}} + K_{\mathrm{w}})q_{\mathrm{w}} + b_{\mathrm{w}} + H_{\mathrm{w}}^T\lambda_{\mathrm{d}} + F_{\mathrm{w}}^T(t)\lambda_{\mathrm{p}} && (30)\\ 0 &= H_{\mathrm{w}}q_{\mathrm{w}} - H_{\mathrm{c}}q_{\mathrm{c}} + (l_1,l_2)^T && (31)\\ 0 &= F_{\mathrm{w}}(t)q_{\mathrm{w}} - b(t, q_{\mathrm{MBS}}(t))\,. && (32) \end{aligned}$$

Mass, damping and stiffness matrices follow from standard computations [24], e. g., it holds

$$M_{\mathrm{c}} = \varrho_{\mathrm{c}}A_{\mathrm{c}}\left(\int_0^L v_{\mathrm{c},i}v_{\mathrm{c},j}\,\mathrm{d}x\right)_{i,j=1}^{N}, \quad K_{\mathrm{w}} = E_{\mathrm{w}}I_{\mathrm{w}}\left(\int_0^L v''_{\mathrm{w},i}v''_{\mathrm{w},j}\,\mathrm{d}x\right)_{i,j=1}^{2N+2}.$$

Furthermore, the constraint matrix H_{c} for the droppers is given by

$$H_{\mathrm{c}}^T = \big(v_{\mathrm{c},i}(x_{\mathrm{d},1}),\ v_{\mathrm{c},i}(x_{\mathrm{d},2})\big)_{i=1}^{N}$$

while the force vector b_{c} contains both gravity and dropper terms (analogously H_{w} and b_{w}),

$$b_{\mathrm{c}} = -\varrho_{\mathrm{c}}A_{\mathrm{c}}g\left(\int_0^L v_{\mathrm{c},i}\,\mathrm{d}x\right)_{i=1}^{N} - H_{\mathrm{c}}^T\begin{pmatrix}(m_{\mathrm{s}} + \frac{1}{2}l_1\,\varrho_{\mathrm{d}}A_{\mathrm{d}})g\\(m_{\mathrm{s}} + \frac{1}{2}l_2\,\varrho_{\mathrm{d}}A_{\mathrm{d}})g\end{pmatrix}.$$

The time dependent constraint vector $F_{\mathrm{w}}(t)$ for the contact of pantograph and catenary, finally, is based on the load distribution (26) and computed by

$$F_{\mathrm{w}}^T(t) = \left(\int_0^L \delta_\epsilon(x - x_{\mathrm{p}}(t))v_{\mathrm{w},i}(x)\,\mathrm{d}x\right)_{i=1}^{2N+2}. \tag{33}$$

Gaussian quadrature provides an efficient and stable way to evaluate (33). Note, that the combination of a cubic Hermite ansatz for w_{w} and the load distribution (25) represents a special type of mixed discretization, compare also the subdomain constraint formulation (17).

How good is the approximation in space using such linear and cubic ansatz functions? Concerning the string model of the carrier, the errors are of order $\mathcal{O}(\Delta x^2)$ as long as the point loads of the droppers act only in some nodes of the grid [24]. Cubic elements, on the other hand, lead in general to errors of order $\mathcal{O}(\Delta x^4)$, but the contact wire discretization will be somewhat worse due to the same point loads. In these nodes, the ansatz is actually too smooth, but we have to compromise here between a conforming ansatz and the Delta functions induced by the droppers.

Looking finally at the structure of the equations, we observe that the carrier matrices in (29) are tridiagonal while the contact wire matrices in (30) are pentadiagonal.

4.3 Semi-discretization by finite differences

To illustrate that the difficulties in the numerical solution of (23) are mainly caused by the PDAE itself and not by a special type of discretization we consider in addition to the FEM discretization (29)–(32) a standard second order finite difference discretization. Finite differences of higher order have been implemented, e. g., by Poetsch/Wallaschek [21].

Consider again the equidistant grid $\{ x_i : 0 \le i \le N+1 \}$ of Sec. 4.2 and denote by $q_{\mathrm{c},i}(t)$ and $q_{\mathrm{w},i}(t)$ the approximations to $w_{\mathrm{c}}(x_i,t)$ and $w_{\mathrm{w}}(x_i,t)$, respectively. The FDM discretization is discussed in detail for the contact wire: First and third derivatives at intermediate points $x_{i+1/2} := \frac{1}{2}(x_i + x_{i+1})$ are approximated by

$$w_{\mathrm{w}}'(x_{i+1/2},t) \doteq \frac{1}{\Delta x}(q_{\mathrm{w},i+1} - q_{\mathrm{w},i})\ , \quad w_{\mathrm{w}}'''(x_{i+1/2},t) \doteq \frac{1}{\Delta x}(q''_{\mathrm{w},i+1} - q''_{\mathrm{w},i}) \quad (34)$$

with

$$q''_{\mathrm{w},i} := \frac{1}{\Delta x^2}(q_{\mathrm{w},i+1} - 2q_{\mathrm{w},i} + q_{\mathrm{w},i-1})\ , \quad (1 \le i \le N)\ .$$

The boundary conditions (3) define $q_{\mathrm{w},0} = q_{\mathrm{w},N+1} = q''_{\mathrm{w},0} = q''_{\mathrm{w},N+1} := 0$.

From the second equation of (2) we obtain by integration over the interval $[x_{i-1/2}, x_{i+1/2}]$

$$\begin{aligned} \int_{x_{i-1/2}}^{x_{i+1/2}} (\varrho_{\mathrm{w}} A_{\mathrm{w}} \ddot{w}_{\mathrm{w}}(x,t) + \beta_{\mathrm{w}} \dot{w}_{\mathrm{w}}(x,t))\,\mathrm{d}x = & \\ & - E_{\mathrm{w}} I_{\mathrm{w}} (w_{\mathrm{w}}'''(x_{i+1/2},t) - w_{\mathrm{w}}'''(x_{i-1/2},t)) + \\ & + T_{\mathrm{w}}(w_{\mathrm{w}}'(x_{i+1/2},t) - w_{\mathrm{w}}'(x_{i-1/2},t)) - \varrho_{\mathrm{w}} A_{\mathrm{w}} g \cdot \Delta x + \\ & + \int_{x_{i-1/2}}^{x_{i+1/2}} (-f_{\mathrm{d},1}^{\mathrm{w}} - f_{\mathrm{d},2}^{\mathrm{w}} + f_{\mathrm{p}}^{\mathrm{w}})\,\mathrm{d}x\ . \end{aligned}$$

Approximating the left hand side by

$$\Delta x \cdot (\varrho_{\mathrm{w}} A_{\mathrm{w}} \ddot{q}_{\mathrm{w},i} + \beta_{\mathrm{w}} \dot{q}_{\mathrm{w},i})$$

and inserting (34) we get a FDM approximation of the form (30) with diagonal matrices

$$M_{\mathrm{w}} := \varrho_{\mathrm{w}} A_{\mathrm{w}} \cdot \Delta x \, I_{N\times N} \ , \quad D_{\mathrm{w}} := \beta_{\mathrm{w}} \cdot \Delta x \, I_{N\times N} \ ,$$

a tridiagonal matrix S_{w} representing the term $T_{\mathrm{w}} w_{\mathrm{w}}''$ and a pentadiagonal matrix K_{w} representing the term $-E_{\mathrm{w}} I_{\mathrm{w}} w_{\mathrm{w}}''''$.

For the FDM discretization the matrices H_{w} and F_{w} in (30) are given by

$$H_{\mathrm{w}}^T := (\, e_{i_1} \, , \, e_{i_2} \,) \ , \quad F_{\mathrm{w}}^T(t) := \left(\int_{x_{i-1/2}}^{x_{i+1/2}} \delta_\epsilon(x - x_{\mathrm{p}}(t)) \, \mathrm{d}x \right)_{i=1}^{N}$$

with the i_j-th unit vectors e_{i_j} and $x_{i_j-1/2} \le x_{\mathrm{d},j} < x_{i_j+1/2}$, $(j = 1, 2)$. The vector

$$b_{\mathrm{w}} := -\varrho_{\mathrm{w}} A_{\mathrm{w}} g \cdot \Delta x - H_{\mathrm{w}}^T \begin{pmatrix} (m_{\mathrm{s}} + \frac{1}{2} l_1 \varrho_{\mathrm{d}} A_{\mathrm{d}}) g \\ (m_{\mathrm{s}} + \frac{1}{2} l_2 \varrho_{\mathrm{d}} A_{\mathrm{d}}) g \end{pmatrix}$$

contains gravitation forces of contact wire, droppers, and suspension clamps.

In the same way the FDM discretization of the first equation in (2) may be written in the form (29) with diagonal matrices M_{c}, D_{c}, and a tridiagonal matrix S_{c}. Finally the active unilateral constraints (5) and (8) are discretized as (31) and (32).

Formally, both FEM and FDM yield a semi-discretized system of the form (29)–(32). Comparing these discretizations the FEM approximation of Sec. 4.2 is seen to be of higher order. At the other hand the diagonal structure of matrices M_{c}, D_{c}, M_{w}, and D_{w} allows some savings of cpu-time in the FDM approach.

5 STABILIZED TIME INTEGRATION OF THE SEMI-DISCRETIZED PDAE

The discretization of the equations of motion (23) is completed by applying techniques from standard DAE theory to the semi-discretized system that was obtained either by FEM or by FDM. In this section we present the 2nd order time discretization schemes that are used in the simulations of Sec. 6 and discuss some details in the handling of the unilateral constraints (5) and (26).

5.1 Index reduction and hidden constraints

Using FEM or FDM the equations of motion are semi-discretized in space, see Sec. 4. The PDE part (2)–(9) describing the catenary results in the DAE (29)–(32), the MBS part (10) that describes the pantograph remains unchanged.

Similar to (23) the semi-discretized system may be written in the compact form

$$\begin{aligned} M_\Delta(q_\Delta)\ddot{q}_\Delta &= A_\Delta q_\Delta + f_\Delta(t,q_\Delta,\dot{q}_\Delta) + G_\Delta^T(t,q_\Delta)\lambda_\Delta \\ 0 &= g_\Delta(t,q_\Delta) \end{aligned} \tag{35}$$

with

$$q_\Delta := \begin{pmatrix} q_{\rm c}(t) \\ q_{\rm W}(t) \\ q_{\rm MBS}(t) \end{pmatrix} ,$$

(see (10) and (29)–(32)). In the benchmark problem of Sec. 2.2 we have

$$\begin{aligned} M_\Delta(q_\Delta) &= \text{blockdiag}\,(\, M_{\rm c}\, ,\, M_{\rm W}\, ,\, m_1\, ,\, m_2\,)\, , \\ A_\Delta &= \text{blockdiag}\,(\, -S_{\rm c}\, ,\, -(S_{\rm W}+K_{\rm W})\, ,\, 0\, ,\, 0\,) \end{aligned}$$

(see (12), (29), (30)) and $\frac{1}{\Delta x}A_\Delta$ approximates the linear differential operator A in (24). Introducing the velocity $v_\Delta := \dot{q}_\Delta$ and accelerations $a_\Delta := \dot{v}_\Delta = \ddot{q}_\Delta$ Eqs. (35) may be rewritten as a first order system that forms an index-3 DAE [11, pp. 463ff].

Any time integration method for standard MBS model equations (10) may be applied to the semi-discretized system (35) (see [11, Chapter VII] for a comprehensive overview). To guarantee numerical stability, all these methods reduce the index of (35) analytically and exploit not only the original constraints $g_\Delta(t,q_\Delta(t)) = 0$ of (35) but also the hidden constraints $\frac{\rm d}{{\rm d}t}g_\Delta(t,q_\Delta(t)) = 0$ (velocity level) and / or $\frac{{\rm d}^2}{{\rm d}t^2}g_\Delta(t,q_\Delta(t)) = 0$ (acceleration level).

In the numerical tests of Sec. 6 we use a generalization of the Gear–Gupta–Leimkuhler formulation [9] that considers simultaneously original and hidden constraints. The hidden constraints are coupled to the equations of motion via auxiliary Lagrange multipliers $\eta,\mu \in \mathbb{R}^{n_\lambda}$. Here, we return to the original problem (2)–(11) where instead of equality constraints $g_\Delta = 0$ unilateral constraints $g_{\Delta,i} \geq 0$ and complementarity conditions $\lambda_{\Delta,i}\cdot g_{\Delta,i} = 0$, $(i=1,\ldots,n_\lambda)$ are given. Since unilateral constraints imply hidden constraints only as long as they are active, we get additional complementarity conditions

$$\eta_i(t)\cdot g_{\Delta,i}(t,q_\Delta) = 0\ ,\ \ \mu_i(t)\cdot g_{\Delta,i}(t,q_\Delta) = 0\ ,\ \ (i=1,\ldots,n_\lambda)\ .$$

The active unilateral constraints and the complementarity conditions for μ are formally summarized to

$$0 = g_\Delta^{(0)}(t,q_\Delta,\mu) = \left(g_{\Delta,i}^{(0)}(t,q_\Delta,\mu)\right)_{i=1}^{n_\lambda}$$

where

$$g^{(0)}_{\Delta,i}(t,q_\Delta,\mu) = \begin{cases} g_{\Delta,i}(t,q_\Delta) & \text{if } g_{\Delta,i}(t,q_\Delta) \le 0 \ , \\ \mu_i(t) & \text{if } g_{\Delta,i}(t,q_\Delta) > 0 \ . \end{cases} \tag{36}$$

The hidden constraints on velocity level and the complementarity conditions for η are summarized as

$$0 = g^{(\mathrm{I})}_\Delta(t,q_\Delta,\dot q_\Delta,\eta) = \Big(g^{(\mathrm{I})}_{\Delta,i}(t,q_\Delta,\dot q_\Delta,\eta)\Big)_{i=1}^{n_\lambda}$$

with

$$g^{(\mathrm{I})}_{\Delta,i}(t,q_\Delta,\dot q_\Delta,\eta) = \begin{cases} \frac{\mathrm{d}}{\mathrm{d}t} g_{\Delta,i}(t,q_\Delta(t)) = \frac{\partial}{\partial t} g_{\Delta,i} + \frac{\partial}{\partial q_\Delta} g_{\Delta,i}\cdot \dot q_\Delta(t) & \text{if } g_{\Delta,i} \le 0 \ , \\ \eta_i(t) & \text{if } g_{\Delta,i} > 0 \ . \end{cases} \tag{37}$$

In the same way the n_λ conditions $g^{(\mathrm{II})}_\Delta(t,q_\Delta,\dot q_\Delta,\ddot q_\Delta,\lambda_\Delta) = 0$ on acceleration level are defined by $\frac{\mathrm{d}^2}{\mathrm{d}t^2} g_\Delta = 0$ with $g^{(\mathrm{II})}_{\Delta,i} := \lambda_{\Delta,i}$ if $g_{\Delta,i} > 0$ such that also the original complementarity conditions for λ_Δ are always satisfied.

With these notations the semi-discretized equations of motion get the form

$$\begin{aligned} M_\Delta(\dot q_\Delta - v_\Delta) &= \Big(\frac{\partial}{\partial q_\Delta} g^{(\mathrm{I})}_\Delta(t,q_\Delta,v_\Delta,\eta)\Big)^T \eta + \Big(\frac{\partial}{\partial q_\Delta} g_\Delta(t,q_\Delta,\mu)\Big)^T \mu \ , \\ M_\Delta(\dot v_\Delta - a_\Delta) &= \Big(\frac{\partial}{\partial \dot q_\Delta} g^{(\mathrm{I})}_\Delta(t,q_\Delta,v_\Delta,\eta)\Big)^T \eta \ , \\ M_\Delta a_\Delta &= A_\Delta q_\Delta + f_\Delta(t,q_\Delta,v_\Delta) + G^T_\Delta(t,q_\Delta)\lambda_\Delta \ , \\ g^{(0)}_\Delta(t,q_\Delta,\mu) &= 0 \ , \\ g^{(\mathrm{I})}_\Delta(t,q_\Delta,v_\Delta,\eta) &= 0 \ , \\ g^{(\mathrm{II})}_\Delta(t,q_\Delta,v_\Delta,a_\Delta,\lambda_\Delta) &= 0 \ . \end{aligned} \tag{38}$$

The auxiliary variables η, μ vanish identically for the analytical solution and are in the size of discretization errors for the numerical solution, the initial values are set to $\eta(0) = \mu(0) = 0$ [7, 9].

For the benchmark problem of Sec. 2.2 Eqs. (38) are substantially simplified since the constraints g_Δ are linear w. r. t. q_Δ such that G_Δ, $\frac{\partial g_\Delta}{\partial q_\Delta}$, $\frac{\partial g^{(\mathrm{I})}_\Delta}{\partial q_\Delta}$, and $\frac{\partial g^{(\mathrm{I})}_\Delta}{\partial \dot q_\Delta}$ are independent of q_Δ and v_Δ and $g^{(0)}_\Delta$, $g^{(\mathrm{I})}_\Delta$, and $g^{(\mathrm{II})}_\Delta$ are linear w. r. t. q_Δ, v_Δ, and a_Δ. Furthermore f_Δ is linear and the mass matrix M_Δ is constant.

5.2 Time discretization

As long as the set of active unilateral constraints $g_{\Delta,i} \ge 0$ does not change system (38) forms an index-2 DAE and may be solved by standard methods like BDF. Similar to the space discretization, we fix the time stepsize Δt and use a 2nd order method. Since two-step methods (like 2nd order BDF) need initial values at $t = 0$ and at $t = \Delta t$ we compute a 2nd order approximation of $q_\Delta(\Delta t)$, $v_\Delta(\Delta t)$, and $a_\Delta(\Delta t)$ by Richardson extrapolation based on backward Euler method with stepsizes Δt and $\Delta t/2$. Alternatively, a half-explicit Euler method may be used for extrapolation.

There is only small damping in the technical system "catenary" and consequently any *numerical* damping may cause wrong simulation results. Numerical damping results from the use of large stepsizes in integrators that are strictly stable at ∞ (BDF, implicit Runge–Kutta methods of Radau IIa type) [23]. Therefore both explicit and most implicit methods have to be applied with rather small stepsizes to (38) (see, however, [12] for a novel integration method that avoids numerical damping completely).

In the numerical tests of Sec. 6, we use two-step BDF for (38) and a half-explicit two-step method for (38) that is based on Störmer's method of 2nd order ([10, Sec. III.10], see also [21]). This half-explicit method may be defined for general problems of the form (38) but to simplify notation we restrict ourselves to the benchmark problem of Sec. 2.2.

For given $q_n^\Delta \approx q_\Delta(t_n)$, $v_n^\Delta \approx v_\Delta(t_n)$, and $v_{n-1}^\Delta \approx v_\Delta(t_{n-1})$, the time step $t_n \to t_{n+1} := t_n + \Delta t$ is defined by:

Step 1 Compute a_n^Δ, λ_n^Δ as solution of the system of linear equations

$$\begin{aligned} M_\Delta a_n^\Delta &= A_\Delta q_n^\Delta + f_\Delta(t_n, q_n^\Delta, v_n^\Delta) + G_\Delta^T(t_n)\lambda_n^\Delta \,, \\ 0 &= g_\Delta^{(\mathrm{II})}(t_n, q_n^\Delta, v_n^\Delta, a_n^\Delta, \lambda_n^\Delta) \,. \end{aligned} \tag{39}$$

Step 2 Set $t_{n+1/2} := t_n + \Delta t/2$ and use Block Gauß elimination to compute $q_{n+1}^\Delta \approx q_\Delta(t_{n+1})$ and $v_{n+1}^\Delta \approx v_\Delta(t_{n+1})$ as solution of the system of linear equations

$$\begin{aligned} M_\Delta\Big(\frac{q_{n+1}^\Delta - q_n^\Delta}{\Delta t} - \frac{1}{2}(v_n^\Delta + v_{n+1}^\Delta)\Big) &= \Big(\frac{\partial g_\Delta^{(\mathrm{I})}}{\partial q_\Delta}(t_{n+1/2})\Big)^T \eta + \Big(\frac{\partial g_\Delta}{\partial q_\Delta}(t_{n+1/2})\Big)^T \mu \,, \\ M_\Delta\Big(\frac{v_{n+1}^\Delta - v_{n-1}^\Delta}{2\Delta t} - a_n^\Delta\Big) &= \Big(\frac{\partial g_\Delta^{(\mathrm{I})}}{\partial \dot q_\Delta}(t_n)\Big)^T \eta \,, \\ 0 &= g_\Delta^{(0)}(t_{n+1}, q_{n+1}^\Delta, \mu) \,, \\ 0 &= g_\Delta^{(\mathrm{I})}(t_{n+1}, q_{n+1}^\Delta, v_{n+1}^\Delta, \eta) \,. \end{aligned} \tag{40}$$

The method (39), (40) is reversible in time. Formally (39) and (40) are implicit w. r. t. all unknowns but for given right hand sides the solution components a_n^Δ, q_{n+1}^Δ, and v_{n+1}^Δ may be obtained very efficiently since M_Δ is tridiagonal (in the FEM case) or even diagonal (in the FDM case). Because only the unknowns λ_n^Δ, μ, and η have to be computed from small dense systems of linear equations, we call (39), (40) a *half-explicit* method.

In the numerical tests we observed an oscillatory instability for damped systems that was fixed substituting $f_\Delta(t_n, q_n^\Delta, v_n^\Delta)$ in (39) by the smoothed term

$$f_\Delta(t_n, q_n^\Delta, \frac{1}{4}(v_{n-1}^\Delta + 2v_n^\Delta + v_{n+1}^\Delta))$$

or (substituting $v_{n+1}^\Delta \to v_{n-1}^\Delta + 2\Delta t\, a_n^\Delta$) by

$$f_\Delta(t_n, q_n^\Delta, \frac{1}{2}(v_{n-1}^\Delta + v_n^\Delta + \Delta t\, a_n^\Delta))\ . \tag{41}$$

With (41) the system (39) is as before linear w. r. t. a_n^Δ, λ_n^Δ since f_Δ is linear in the benchmark problem.

The stepsize Δt of the half-explicit method has to satisfy $\Delta t \le c \cdot \Delta x^2$ to guarantee stability since the largest eigenvalue of matrix $M_\Delta^{-1} A_\Delta$ is of size $\mathcal{O}(\Delta x^{-4})$. In the numerical tests of Sec. 6 we use stepsizes $\Delta t = c \cdot \Delta x^2$ with an appropriate constant $c > 0$ both for the half-explicit method (to avoid instability) and for BDF (to avoid numerical damping and instability).

5.3 Systems with varying structure

The time discretization method has to be extended by an algorithm to handle changes of the set of active unilateral constraints. In each time step $t_n \to t_{n+1}$, the set of active constraints at t_{n+1} is determined iteratively. This algorithm is discussed for the half-explicit method (39), (40), it may be carried over straightforwardly to BDF and other methods.

We denote by

$$J_{n+1} := \{\, i \,:\, 1 \le i \le n_\lambda\,,\ g_{\Delta,i}(t_{n+1}, q_{n+1}^\Delta) = 0\,\}$$

the (a priori unknown) index set of active constraints at t_{n+1}. In (39) and (40) the definitions (36) and (37) of $g_\Delta^{(0)}$, $g_\Delta^{(\mathrm{I})}$, and $g_\Delta^{(\mathrm{II})}$ are slightly modified substituting the conditions "if $g_{\Delta,i} \le 0$" and "if $g_{\Delta,i} > 0$" by "if $i \in J_{n+1}$" and "if $i \notin J_{n+1}$", respectively.

Most often the set of active constraints does not change in a time step $t_n \to t_{n+1}$. We therefore start with method (39), (40) and $J_{n+1} := J_n$ to get a_n^Δ, λ_n^Δ, q_{n+1}^Δ, and v_{n+1}^Δ.

If these vectors are consistent with the unilateral constraints, i. e. if

$$g_{\Delta,i}(t_{n+1}, q_{n+1}^\Delta) \ge 0\,,\ \ \lambda_{n,i}^\Delta \ge 0\,,\ (i = 1, \ldots, n_\lambda)\,,$$

then the time step $t_n \to t_{n+1}$ is completed successfully and the integration may be continued with time step $t_{n+1} \to t_{n+2}$.

If there is an $i \notin J_{n+1}$ with $g_{\Delta,i}(t_{n+1}, q_{n+1}^\Delta) < 0$ then the i-th unilateral constraint has become active in time step $t_n \to t_{n+1}$, the index "i" has to be added to J_{n+1} and the time step $t_n \to t_{n+1}$ is repeated.

If there is an $i \in J_{n+1}$ with $\lambda^{\Delta}_{n,i} < 0$ then the i-th unilateral constraint has become inactive in time step $t_n \to t_{n+1}$, the index "i" has to be deleted from J_{n+1} and the time step $t_n \to t_{n+1}$ is repeated.

This algorithm is robust and efficient. Note, that we do not determine exactly the time instant $t^* \in [t_n, t_{n+1}]$ where an inactive constraint gets active or vice versa. In each single time step $t_n \to t_{n+1}$ the set of active constraints is considered to be fixed. This is justified by the very small time stepsize, by the low order of the method, and by the large error of the physical model.

An inactive unilateral constraint that gets active corresponds in the physical model to two bodies getting in contact and results typically in an impact in the system. Implicitly, we have assumed by $g^{(\mathrm{I})}_{\Delta} = 0$ in (40) that these impacts are inelastic [15].

6 SIMULATION RESULTS

The following selection of simulation results shows some typical properties of the benchmark problem pantograph/catenary and illustrates the numerical techniques discussed above. We use the benchmark data as specified in Sec. 2.2 and discretize carrier and contact wire by an equidistant grid of $N + 1 = 500$ intervals.

Space discretization	Carrier		Contact wire	
	$\omega_{\max}$	$\omega_{\min}$	$\omega_{\max}$	$\omega_{\min}$
FEM	$2.1793 \cdot 10^3$	3.9528	$5.9257 \cdot 10^4$	2.9631
FDM	$1.2582 \cdot 10^3$	3.9528	$4.8088 \cdot 10^3$	2.9631

Table 1. Eigenfrequencies of carrier and contact wire in Hz for $N + 1 = 500$ intervals.

Table 1 gives maximum and minimum frequencies of the subsystems in the undamped case. The low frequencies of FEM and FDM space discretization are in good agreement, but the conforming cubic FEM approach for the contact wire leads to a much higher maximum frequency. Concerning the time integration by the time reversible half-explicit method of Sec. 5.2, this means that the stepsize Δt is restricted to $6.6 \cdot 10^{-5}$ s in case of the FDM grid and to $5.3 \cdot 10^{-6}$ s in case of the FEM grid. With respect to efficiency, the combination of FEM discretization and time reversible integration suffers thus from a more than ten times smaller stepsize.

The initial state of the catenary due to the gravity and the constraints (5) and (26) is displayed in Fig. 5. Here, the pantograph speed was chosen as $v_\mathrm{p} = 32\,\mathrm{m/s}$. The corresponding time integration results are shown in Fig. 6. With respect to position variables, the solution remains comparatively smooth. On the other hand, with increasing time the constraint forces start oscillating though the unilateral constraints are always active, i.e., there is no loss of contact between pantograph head and catenary and the droppers do not slacken. Looking at the accuracy, the difference between FDM and FEM space discretization is negligible here, and also the time integration by second order BDF or the half-explicit method yields comparable results. The solution in Fig. 6 was computed using a constant stepsize of $\Delta t = 5 \cdot 10^{-5}\,\mathrm{s}$ and either BDF-2 for the FEM discretization or the time reversible half-explicit method for the FDM grid.

If we rerun the simulation with increased speed $v_\mathrm{p} = 48\,\mathrm{m/s}$, the solution behavior changes considerably, Fig. 7. First, there is a very high sensitivity of the solution with respect to the initial values. In order to avoid an immediate loss of contact between pantograph head and catenary, it was necessary to change the choice (13) for the initial pantograph position to

$$w_{\mathrm{p},1}(0) = w_{\mathrm{p},2}(0) + 0.002\,\mathrm{m}\,.$$

Second, the oscillations in the constraint forces grow strongly. In particular, the constraint force λ_p between pantograph head and catenary is characterized by very sharp peaks and much higher maximum values. This is partly due to a third phenomenon, the slackening of the second dropper. The pantograph passes the first dropper at time $t = 0.0729\,\mathrm{s}$, which leads to a distinct minimum of the constraint force $\lambda_{\mathrm{d},1}$. At $t = 0.2604\,\mathrm{s}$, the second dropper is reached, and now $\lambda_{\mathrm{d},2}$ tends to zero whence the unilateral constraint (5) becomes inactive, the dropper slackens. This event was localized by the technique outlined in Sec. 5.3, and the integration was continued without the corresponding constraint equation until the constraint $\Delta_{\mathrm{d},2} \geq 0$ became active again. Note, that space discretization by either FEM or FDM is here clearly superior to a modal approach since it offers a straightforward handling of such discontinuities. In real life simulations, slackening of droppers happens frequently and thus appropriate numerical techniques are essential.

Finally, we remark that also for $v_\mathrm{p} = 48\,\mathrm{m/s}$, the difference between space discretization by either FEM of FDM as well as the difference between time integration by either BDF or the half-explicit method were very small. Furthermore, in all simulations the influence of viscous damping in terms of factors β_c and β_w, cf. (2), was negligible.

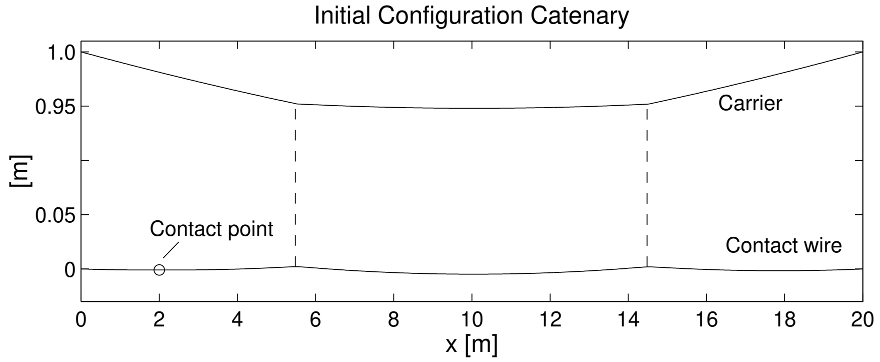

Fig. 5. Initial configuration of the catenary.

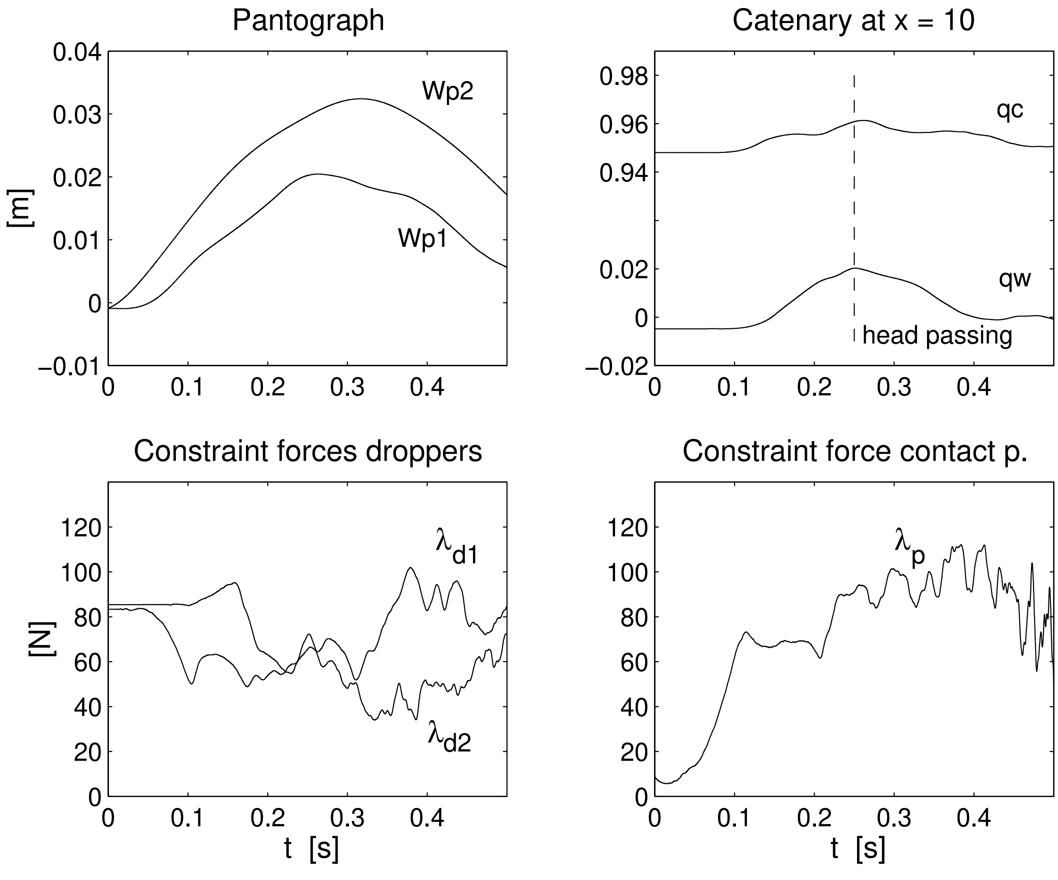

Fig. 6. Time integration results for $v_{\mathrm{p}} = 32\,\mathrm{m/s}$.

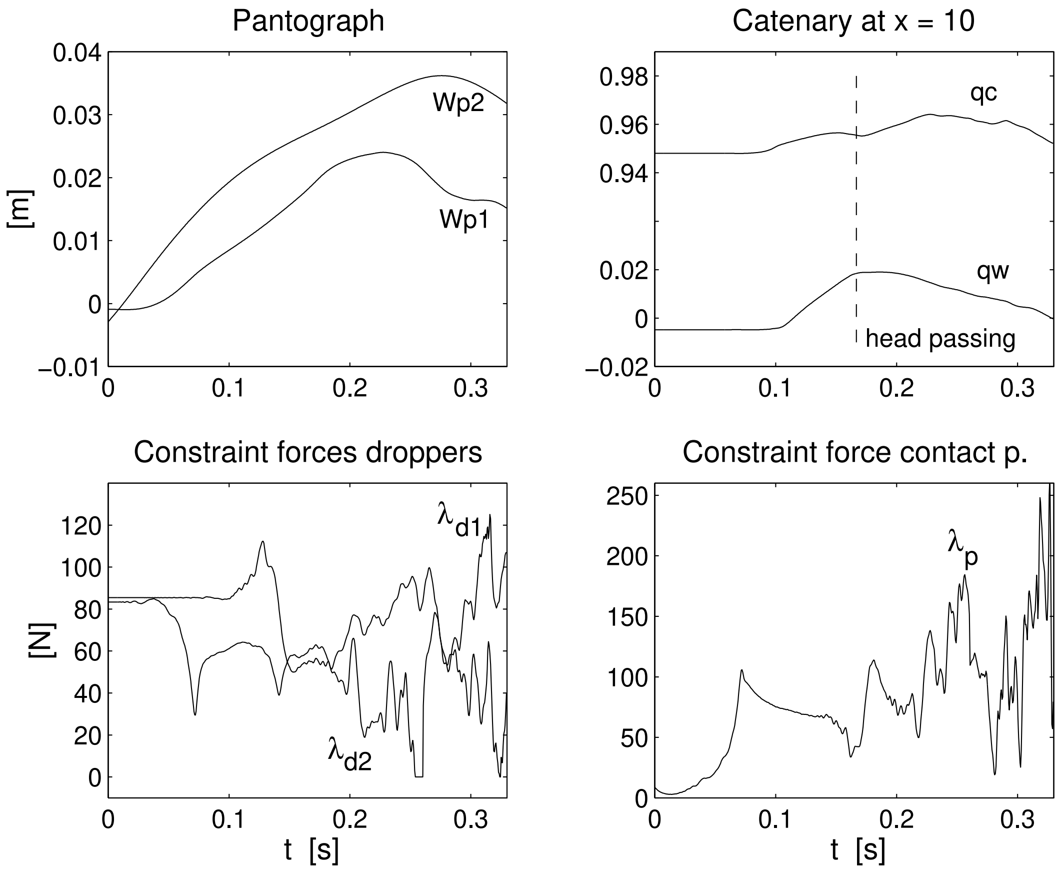

Fig. 7. Time integration results for $v_{\mathrm{p}} = 48\,\mathrm{m/s}$. Note that the second dropper slackens when the pantograph head is passing at time $t = 0.2604\,\mathrm{s}$. The corresponding constraint force $\lambda_{\mathrm{d},2}$ equals zero for a short time intervall.

7 SUMMARY

Simulation plays a very important role in the analysis of the pantograph/catenary interaction as well as in the design of innovative pantograph concepts. Clearly, the quality of any simulation result depends on the model, the available data, and the numerical solution techniques. But in case of complex technical applications like the system of pantograph and catenary, there is not only one model equation and one or two numerical schemes. Instead, several physical processes are described by corresponding differential equations (PDE's and DAE's), and the mutual coupling becomes the most crucial part.

Though tempting, we do here not advocate approaches where modelling and numerical solution are intertwined, e. g., by first discretizing some subsystems in space and then setting up the overall model. The alternative we propose is the mathematical model of Sec. 2, a partial differential-algebraic equation or PDAE which comprises all equations and coupling conditions *before discretization*. Like the descriptor form in rigid body systems, this approach offers great flexibility in the handling of additional subsystems and does not exclude any numerical technique a priori.

It turns out that the PDAE of Sec. 2 does not fit into the framework developed so far in the literature. On the other hand, mechanical systems including deformable bodies lead quite naturally to constraints on some boundary or subdomain, and hence the pantograph PDAE represents a typical example for this broad class of applications. We hope that the simple benchmark problem introduced in Sec. 2.2 will serve as a reference to study such problems. Note that the discussion in Sec. 3 shows that one has to be careful when applying standard DAE techniques like differentiation of constraints.

The numerical methods outlined in Secs. 4 and 5 realize a MOL type approach. Alternatives like Rothe's method based on the PDAE formulation have not been investigated so far. We want to stress in this context that space and time discretization should preserve as much information as possible. For this purpose, we presented a novel half-explicit integration method which is reversible in time. Its application to the semi-discretized PDAE involves no numerical damping, in contrast to standard methods like BDF.

Finally, the simulation results for the benchmark problem illustrate that the constraint between pantograph and catenary and the corresponding constraint force is the most important part in both model formulation and numerical solution. Concerning the latter, we did not use any adaptivity in space or time, a topic which definitely needs further attention.

ACKNOWLEDGEMENTS

We acknowledge gratefully the stimulating discussions at a workshop on MBS with elastic bodies that was held in October, 1997, at the Institute of Robotics and System Dynamics, DLR Oberpfaffenhofen. In particular we would like to thank our colleagues Dipl.-Ing. G. Poetsch (DB AG), Dr.-Ing. D. Sachau (DLR), and Dipl.-Ing. A. Veitl (DLR) for providing detailed information about the system pantograph/catenary and about the background in classical mechanics. Various figures in the present paper are based on drawings by G. Poetsch, A. Veitl, and cand. math. D. Jäger (FH Regensburg). Finally, we are greatly indebted to Prof. P. Rentrop (TU Darmstadt) and Prof. W. Kortüm (DLR) for their permanent support of our activities.

REFERENCES

1. D. Braess. *Finite Elemente.* Springer–Verlag, Berlin, 1991.
2. K.E. Brenan, S.L. Campbell, and L.R. Petzold. *Numerical solution of initial–value problems in differential–algebraic equations.* SIAM, Philadelphia, 2nd edition, 1996.
3. S.L. Campbell and W. Marszalek. The index of an infinite dimensional implicit system. Technical Report 96/1996, North Carolina State University Raleigh, Department of Mathematics, May 1996, to appear in: Mathematical Modelling of Systems.
4. S.L. Campbell and W. Marszalek. DAEs arising from traveling wave solutions of PDEs. *J. Comp. Appl. Math.*, 82:41–58, 1997.
5. E. Eich-Soellner and C. Führer. *Numerical Methods in Multibody Dynamics.* Teubner–Verlag, Stuttgart, 1998.
6. W. Fischer. *Eine Methode zur Berechnung des Schwingungsverhaltens von Kettenwerk und Stromabnehmer bei hohen Zuggeschwindigkeiten.* PhD thesis, TH Darmstadt, 1975.
7. C. Führer and B. Leimkuhler. Numerical solution of differential–algebraic equations for constrained mechanical motion. *Numer. Math.*, 59:55–69, 1991.
8. C.W. Gear. Differential-algebraic equation index transformations. *SIAM J. Sci. Stat. Comput.*, 9:39–47, 1988.
9. C.W. Gear, G.K. Gupta, and B. Leimkuhler. Automatic integration of Euler–Lagrange equations with constraints. *J. Comp. Appl. Math.*, 12&13:77–90, 1985.
10. E. Hairer, S.P. Nørsett, and G. Wanner. *Solving Ordinary Differential Equations. I. Nonstiff Problems.* Springer-Verlag, Berlin Heidelberg New York, 2nd edition, 1993.
11. E. Hairer and G. Wanner. *Solving Ordinary Differential Equations. II. Stiff and Differential-Algebraic Problems.* Springer-Verlag, Berlin Heidelberg New York, 2nd edition, 1996.
12. M. Hochbruck and Ch. Lubich. A Gautschi–type method for oscillatory second-order differential equations. Technical Report Nr. 91, University of Tübingen, SFB 382, January 1998.
13. N. Kikuchi and J. Oden. *Contact Problems in Elasticity.* SIAM, Philadelphia, 1988.
14. M. Link and B. Nowak. Zur dynamischen Analyse des Systems Stromabnehmer und Fahrleitung, dargestellt am Beispiel des Intercity–Experimental. VDI–Berichte, Nr. 503, S. 245–261, 1986.

15. P. Lötstedt. Mechanical systems of rigid bodies subject to unilateral constraints. *SIAM J. Appl. Math.*, 42:281–296, 1982.
16. Ch. Lubich and A. Ostermann. Runge–Kutta methods for parabolic equations and convolution quadrature. *Mathematics of Computation*, 60:105–131, 1993.
17. W. Lucht and K. Strehmel. Discretization based indices for semilinear partial differential algebraic equations. Technical Report 40(1997), Martin–Luther–University Halle, Department of Mathematics and Computer Science, 1997.
18. W. Lucht, K. Strehmel, and C. Eichler-Liebenow. Linear partial differential algebraic equations. Part I: indexes, consistent boundary/initial conditions. Technical Report 17(1997), Martin–Luther–University Halle, Department of Mathematics and Computer Science, 1997.
19. K. Petri. *Vergleichende Untersuchung von Berechnungsmodellen zur Simulation der Dynamik von Fahrleitung–Stromabnehmer–Systemen.* PhD thesis, Heinz–Nixdorf–Institut, Universität–GH Paderborn, Germany, 1996.
20. G. Poetsch, J. Evans, R. Meisinger, W. Kortüm, W. Baldauf, A. Veitl, and J. Wallaschek. Pantograph/catenary dynamics and control. *Vehicle System Dynamics*, 28:159–195, 1997.
21. G. Poetsch and J. Wallaschek. Simulating the dynamic behaviour of electrical lines for high-speed trains on parallel computers. In *Proceedings of the International Symposium on Cable Dynamics*, pages 565–572, A. I. M. Liège, 1995.
22. B. Simeon. DAE's and PDE's in elastic multibody systems. *Numerical Algorithms*, accepted for publication, 1997.
23. B. Simeon. Order reduction of stiff solvers in elastic multibody systems. *Applied Numerical Mathematics*, accepted for publication, 1997.
24. G. Strang and G. Fix. *An Analysis of the Finite Element Method.* Prentice Hall, Englewood Cliffs, 1973.
25. O.C. Zienckiewicz and R.L. Taylor. *The Finite Element Method.* Mc Graw Hill, London, 1994.